

Fig. 2: Schematic showing motor power flow

Thermal resistance values for all conduction paths within the motor are calculated from motor dimensions and material data. The accuracy of the calculation is dependent upon knowledge of the various thermal contact resistances between components within the motor, e.g. housing to lamination interface, slot-liner to lamination interface. Such resistances occur due to contact between solid surfaces taking place at limited numbers of high spots, the adjacent voids usually being filled with air. There has been much experimental work on the prediction of contact resistance [9, 12, 15]. The Motor-CAD online help system summarises this literature to include guidance on effective gaps to be expected with different material types, interface pressures and surface roughness. Motor-CAD combined with motor test data also forms an effective parameter identification tool. This technique can be used to estimate the gaps within the machine which are physically impossible to measure and to quantify the effects of winding impregnated air pockets.

Cross-Section Editor:

Radial & axial cross-section editors are used for dimensional data input (Figs 3 to 5). Figs 3 & 4 show a 80mm diameter concentrated winding motor design, in this case having 12 slots and 8 poles. Fig 5 shows a traditionally wound motor having 18 slots and 6 poles. It has the same diameter and axial length as the concentrated wound motor, however, its overall length is 30% longer to accommodate the longer end-turns. The visual feedback produced helps the user gain an insight about the importance of the various heat paths within the motor. Thermal resistance is proportional to length and inversely proportional to cross-sectional area and thermal conductivity. The feedback also reduces the incidence of input errors.

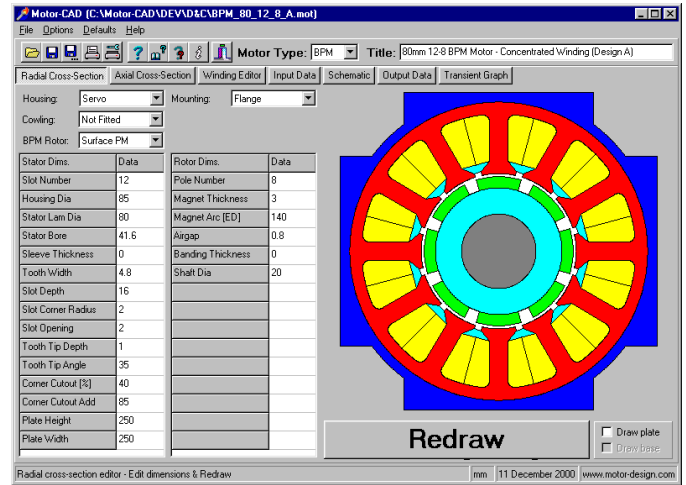


Fig. 3: Motor radial cross-section editor showing a 80mm diameter concentrated winding motor design

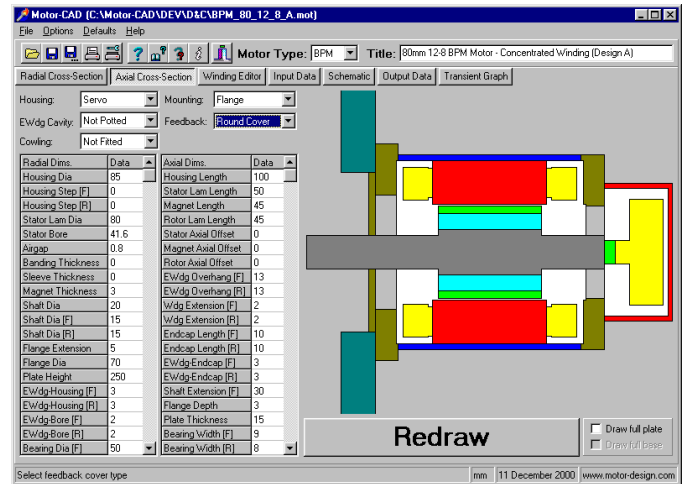


Fig. 4: Motor axial cross-section editor showing a 80mm diameter concentrated winding motor design

Winding Design:

The winding is modelled using several layers of copper, wire insulation and inter-conductor insulation (impregnation and/or air) together with a slot-liner and a slot-liner-lamination interface gap (Figs 6 & 7). The number of layers and copper to insulation thickness ratio is set by wire diameter, number of turns and subsequent slot-fill. The winding diagrams are useful for gaining a visual indication of the slot-fill that can be achieved using various winding techniques. For instance the winding shown in Fig 6 is for a traditional winding in which the coils are inserted into the slots through the slot openings. This is the winding used in the motor shown in Fig 5. Fig 7 shows the increased slot fill that can be achieved using a more modern concentrated winding in which the non-overlapping coils are precision wound directly onto a segmented tooth, the teeth then being joined together to form a wound stator [4]. This is the winding used in the motor shown in Figs 3 & 4.

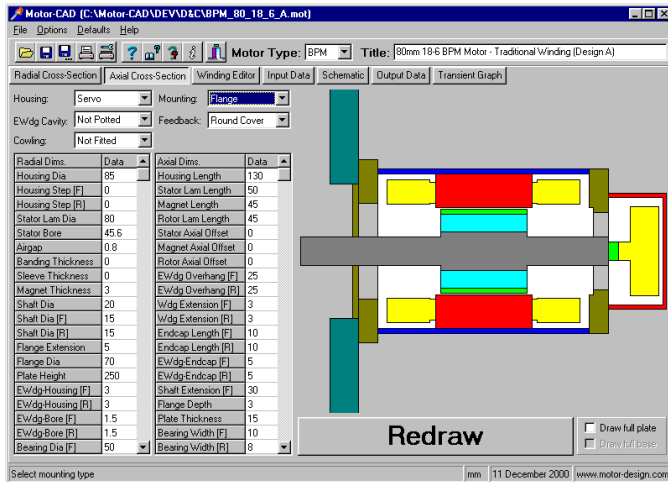


Fig. 5: Motor axial cross-section editor showing a 80mm diameter traditionally wound motor design

Concentrated winding techniques:

Fig 6 shows a traditional winding in which the coils are inserted into the slots through the slot openings. This has a slot-fill limit of around 55% (based on round covered conductors and slot area available for winding after liner insertion). Fig 7 shows the increased slot fill that can be achieved using a more modern concentrated winding in which the non-overlapping coils are precision wound directly onto a segmented tooth and the teeth are subsequently joined together to form a wound stator [4]. Slot fills of around 80% can be achieved using this technique.

The windings shown in Figs 6 & 7 are used in the motors shown in Fig 5 & 4 respectively. It is seen that the non-overlapping winding benefits from having a shorter end-winding length. This also gives a reduction in resistance and copper loss. For example, in the case of the 80mm diameter motor reported here, the 12-slot 8-pole concentrated winding design has a 100mm overall length compared to 130mm for the 18-slot 6-pole traditionally wound motor. It also produces 34% more torque for the same temperature rise. A similar design study has been carried using a 36-slot, 6-pole traditionally wound motor and a 12-slot, 8-pole concentrated wound motor, both having a 160mm housing diameter and the same active length. The two stator lamination designs are shown in Fig 9. In this case the 12-slot design has a overall length of 190mm compared to 230mm, but the torque increase for a given temperature rise is only 8%. The reduced improvement is largely due to the fact that the 36-slot motor has 80% more total slot periphery than the 12-slot motor to dissipate its copper. In the case of the 80mm motors, the 18-slot motor has only a 16% benefit in terms of total slot periphery compared to the 12-slot motor. For this reason a larger slot number may be beneficial in the 160mm motor, probably a 16-slot 18-pole or a 24-slot 16-pole design. The 16-slot 18-pole benefits from not requiring skew, the 24-slot 16-pole and 12-slot 8-pole designs needing to be skewed by half a

slot pitch. The increased pole number would however lead to increased iron loss, although these are closer to the outside of the motor and would be easier to dissipate. These design possibilities will be investigated in the near future.

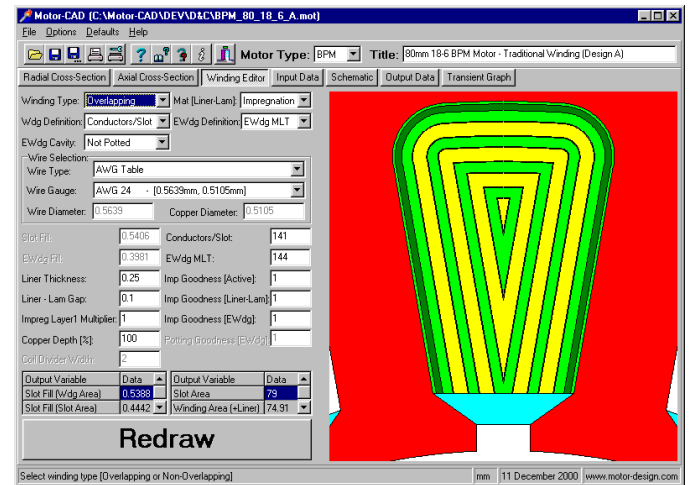


Fig. 6: Winding model showing copper/insulation layers in a traditional winding where are coils inserted into slots

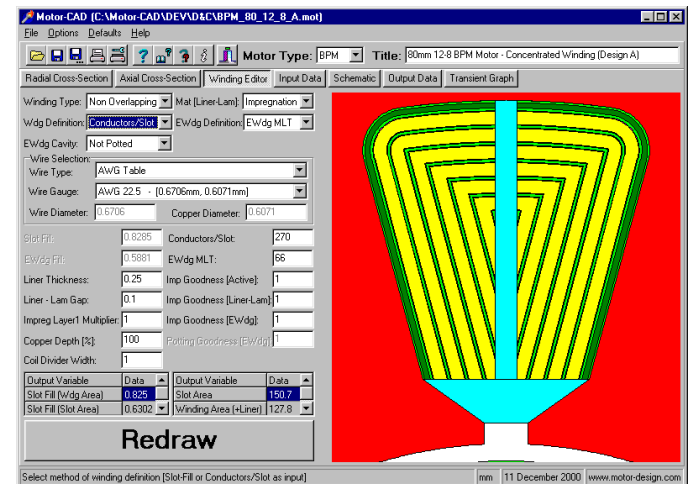


Fig. 7: Winding model showing the high slot-fills achievable in a precision wound non-overlapping winding

Additional methods to increase the winding dissipation include improved winding impregnation techniques and potting of the end-windings. Vacuum impregnation can eliminate air pockets within the winding. For instance the winding shown in Figs 5 & 6 benefit from a decrease in temperature rise of around 9% when the motors are perfectly impregnated compared to a 50% impregnated motor. The previous examples use a traditional impregnation material having a thermal conductivity of 0.2W/m°C. However, new high temperature impregnation and potting materials are now available which have thermal conductivities of around 1W/m°C. If one of the new materials were to be used in the two designs shown in Figs 5 & 6, a reduction in temperature rise of between 6% and 8% could be expected. If the end-

windings were potted, a reduction in temperature rise of between 14% and 16% would be expected.

Thermal Mathematical Models:

Motor-CAD features efficient, accurate and robust mathematical algorithms for forced & natural convection, radiation and conduction. The particular convection model used for the various surfaces throughout the motor are automatically selected from a library of proven laminar and turbulent convection correlations [12-20]. Correlation formulations for open and closed channels and external surfaces of various shapes and orientations are included. Totally enclosed non-ventilated (TENV) and totally enclosed fan cooled (TEFC) forms of cooling are included. However, as the correlation formulations used are based upon dimensionless analysis of heat transfer [15], they are also applicable to liquid cooling methods such as housing water jackets, shaft spiral grooves, wet rotor and wet stator cooling techniques. These are included in Motor-CAD. Rotation effects on convection cooling in the airgap are included within the model [19-20].

Fin Design:

The fin design is often given little attention in servo motors as they traditionally do not have a shaft mounted fan because they are intended to operate down to zero speed. The radial fin design shown in Fig 8 can however be used to increase the amount of natural convection from the housing [10,11,23]. In the case of the 80mm diameter motors presented earlier, a reduction in temperature rise of around 10% can be achieved by adopting a radial fin design. There are special radial fin designs which allow similar dissipation when the motor is mounted vertically as when mounted horizontally [10,23].

External blower units are sometimes used to increase the output from servo motors [24]. If these are to be used, then one of the axial fin designs shown in Fig 9 would be beneficial.

Mounting Arrangement:

The mounting arrangement can have a significant impact on the thermal behaviour of the motor. In the servo motors shown in this paper, between 35 - 50% of the total loss is dissipated through the flange, the larger value being in the smaller motors. Such high figures are not uncommon as manufactures tend to use larger cooling plates than the standard plate sizes recommended by NEMA [22]. A motor must de-rate if it is unable to dissipate such powers into the device it is connected to.

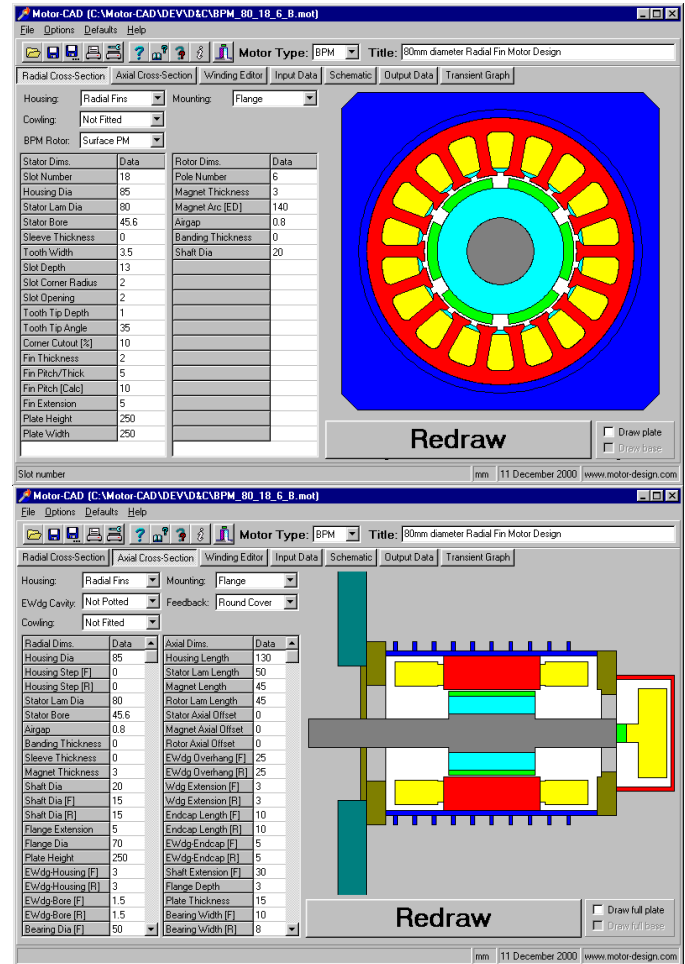


Fig 8: Motor with a radial fin design

Feedback Devices & Integrated Motors:

When an encoder is used as a feedback device then this should be included in the model as they typically have temperature limits of between 80°C and 100°C. The encoder model used in Motor-CAD is shown in Figs 1 & 4. The encoder model can also be adapted to predict the temperature rise of control and power electronics attached to the rear of motors in integrated motor drives [21].

Magnet Temperature Limit:

The magnet temperature is a key item to be calculated in permanent magnet motors, especially when Nd-Fe-B magnets are being used. This is because they are more sensitive to demagnetisation at elevated temperatures than Sm-Co. They also have a larger negative temperature coefficient of remanence which can lead to a significant reduction in torque/amp (Kt) at high temperatures. The trend is that the higher remanence Nd-Fe-B materials which are suited to high power densities also have a lower BH knee value so are more prone to demagnetisation. However new grades of Nd-Fe-B are emerging that have relatively high remanence (1.19T) and linear 3rd quadrant BH characteristics up to 180°C [25]. It is

reassuring that the magnets are somewhat isolated from the main sources of loss (i.e. the stator copper and iron loss), so that under a severe overload condition, the magnet temperature rise is much slower than that of the stator components (Fig 11).

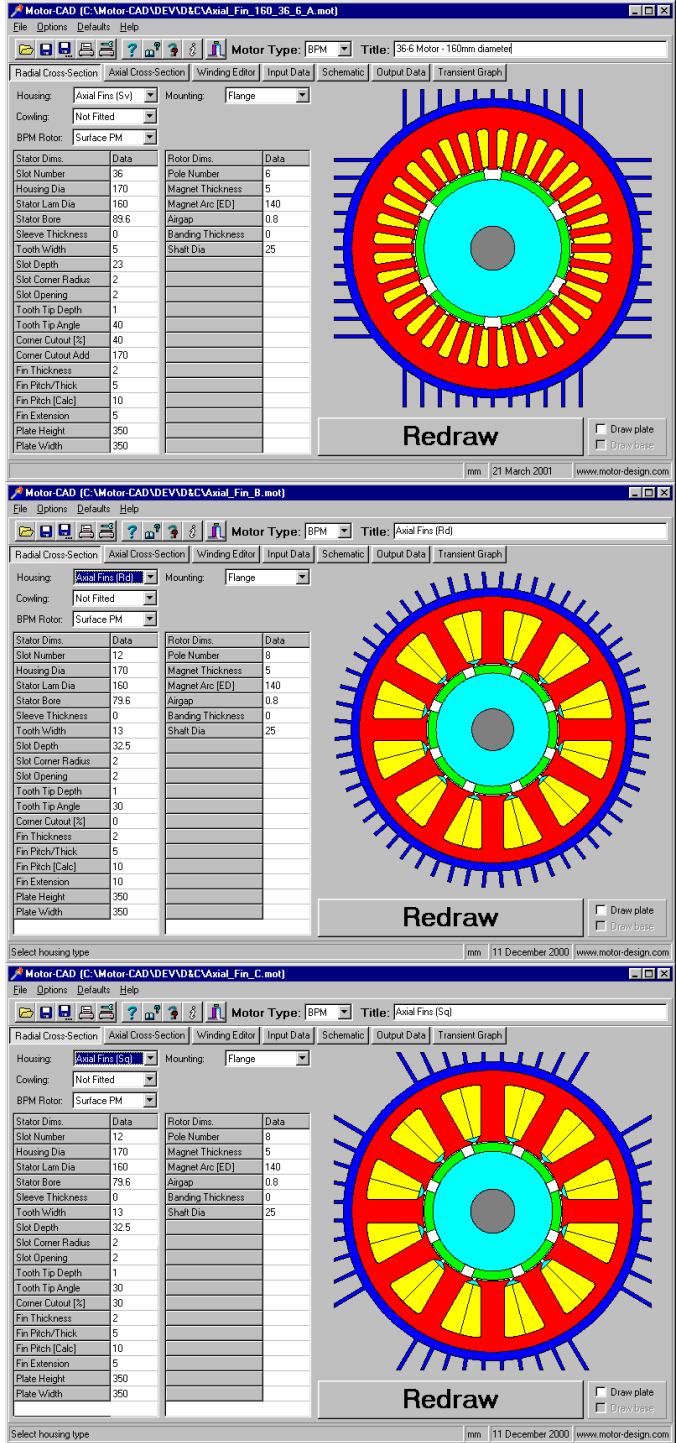


Fig 9 Examples of axial fin types available in Motor-CAD

Transient Analysis:

When carrying out transient analysis, thermal capacitances are connected to each of the nodes within the schematic shown in Fig 1. Each capacitance is calculated from the specific heat capacity and weight of the relevant motor components. The resulting set of partial differential equations are integrated to obtain the thermal transient characteristics.

Typical transient graphs are shown in Figs 10 & 11. Fig 10 shows the thermal transient produced when a motor is run at constant torque until the motor reaches its steady state temperature. It also shows the typical level of correspondence expected between measured and calculated transient characteristics when using Motor-CAD. It is also interesting to note that as with most motor rating tests, the motor current must be varied throughout the test to accommodate the torque constant (Kt) and iron losses which both reduce as the magnets heat up. These effects, in addition to the increase in winding resistance with temperature and the variation in losses with speed, are all taken account of within the program.

The transient graph shown in Fig 11 shows changes in temperature of the different motor components when driving a complex duty-cycle load. The duty-cycle editor used to describe the load is shown in Fig. 12. Duty-cycle analysis is essential in the majority of servo applications if the motor is to be driven to full potential without over-heating. This is illustrated in Figs 10 and 11 as the same motor is used for both calculations. When run continuously at rated torque the winding takes nearly 2 hours to reach its steady-state temperature. However when a severe duty cycle is used to load the machine, the same temperature is reached in around 100 seconds.

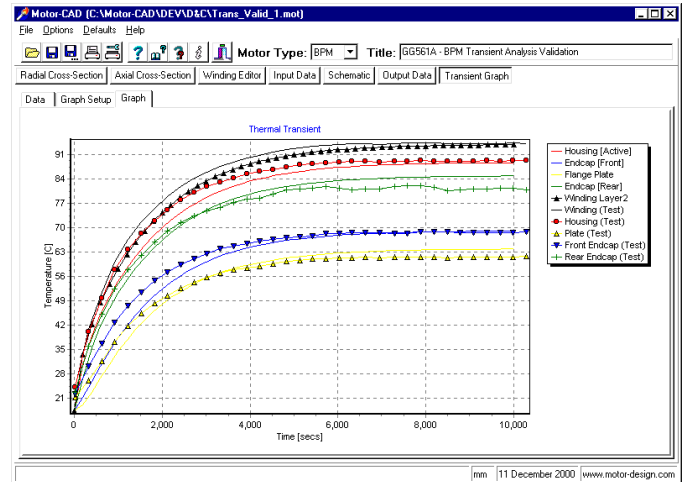


Fig. 10: Comparison of measured and calculated thermal transient for a small servo motor

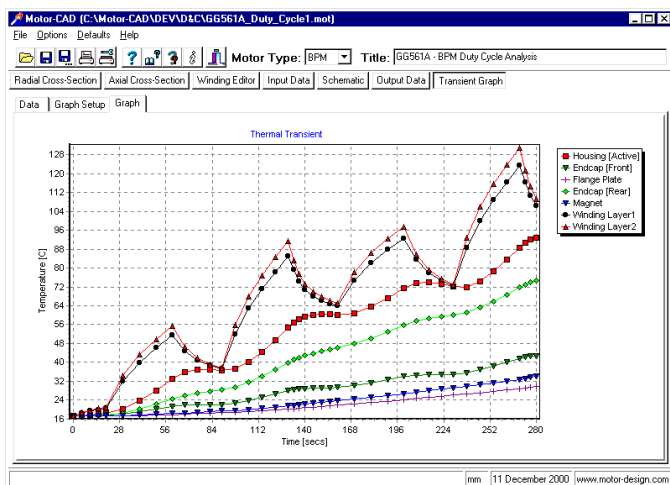


Fig. 11: Thermal transient for a small servo motor operating a duty cycle type load (load shown in Fig 12).

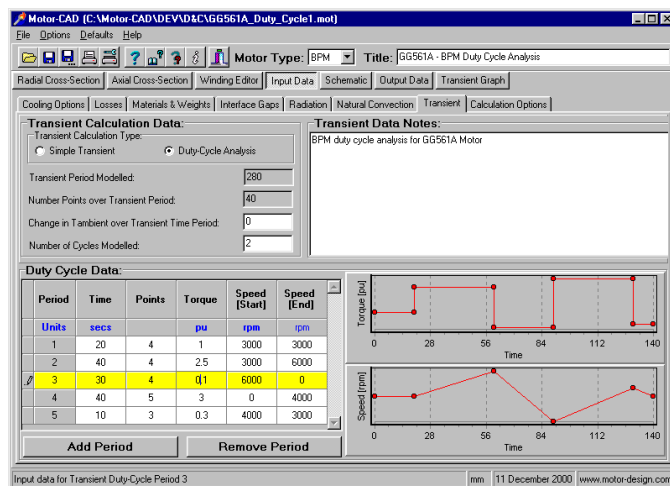


Fig. 12 Duty-cycle load editor

Conclusions

This paper clearly demonstrates the advantages that can be gained from properly analysing the thermal characteristics of electric motors at the design stage. Motor-CAD has been developed as a tool to assist the designer in this complex and important area of design. Some examples of how thermal analysis can aid the miniaturisation of permanent magnet motors have been shown, supported by data where appropriate.

Motors-CAD transient calculation capabilities have been demonstrated with test data. If a motor is to be driven to full potential without over-heating, the importance of carrying out transient duty-cycle analysis has also been shown.

Acknowledgement

Dr Eric So, Vickers Systems Division

References

- [1] AC Servo Drive Σ Series, Yaskawa Product Brochure No. CHE-5800-18B
- [2] Technology Update - Servo Motors Double the Power Density, Drives & Controls, Jan. 2000
- [3] Compact Servos Boost Throughput, Drives & Controls, Sept. 2000
- [4] Compact Servo Motors, OEM Design, June 1995
- [5] AC motors are a third of the size, Drives & Controls Oct. 2000
- [6] Swedes Shrink Servomotors, Drives & Controls, April. 2000
- [7] Hendershot, J.R., Miller, T.J.E.: Design of Brushless Permanent-Magnet Motors, Magna Physics & Oxford Science Publications, 1994
- [8] Hanselman, D.C.: Brushless Permanent-Magnet Motor Design, McGraw-Hill, 1994
- [9] Hamdi, E.S.: Design of Small Electrical Machines, Wiley, 1994.
- [10] Staton, D.A., So E.: Determination of Optimal Thermal Parameters for Brushless Permanent Magnet Motor Design, IEEE-IAS Conference, St.Louis, Oct. 1998
- [11] Staton, D.A.: Thermal Analysis of Naturally Ventilated Servo Motor Housings, 5th International Flotherm User Conference, Paris, 16-19 Sept. 1996.
- [12] Ozisik, M.N.: Heat Transfer - A Basic Approach, McGraw Hill, 1995.
- [13] Simonson, J.R.: Engineering Heat Transfer, Macmillan, 1988.
- [14] White, F.M., Heat and Mass Transfer, Addison-Wesley.
- [15] Janna, W.S., Engineering Heat Transfer (S.I. Edition), Van Nostrand Reinhold (International), 1988
- [16] Bejan, A., Heat Transfer, John Wiley & Sons, Inc., 1993
- [17] Incropera, F.P., DeWitt, D.P., Introduction to Heat Transfer, John Wiley & Sons, 1990
- [18] Mellor, P.H., Roberts, D., Turner, D.R.: Lumped Parameter Thermal Model for Electrical Machines of TEFC Design. IEE Proc-B, Vol. 138, No. 5, Sept 1991.
- [19] Taylor, G.I.: 'Distribution of Velocity and Temperature between Concentric Cylinders', Proc Roy Soc, 1935, 159, PtA, pp 546-578
- [20] Gazley, C.: 'Heat Transfer Characteristics of rotating and axial flow between concentric cylinders', Trans ASME, Jan 1958, pp.79-89.
- [21] Technology Update, Drives & Controls, May 2000
- [22] Nema Standards:, Publication No. MG7, Revision Jan. 26, 1993.
- [23] Unimotor knocks the competition out cold, Torqueback magazine, Control Techniques Dynamics Ltd, Vol 1, Issue 3.
- [24] Fan cowlings boost torque by up to 87%, Drives & Controls, Oct. 1999.
- [25] Sumitomo Numax Catalogue, 1999